Renewable Energy and Power Quality Journal
https://repqj.com/index.php/repqj/index
RE&PQJ, Vol. 24, No. 4, 2026

Numerical Modeling to Optimize the Parameters for Ga_2CeCl_6 based Solar Cell

Sumeet Kumar*

Department of Computer Science and Engineering, School of Engineering Sciences and Technology, Jamia Hamdard, New Delhi, 110062, Delhi, India.

*Corresponding Author: Sumeet Kumar, sumeet.kumar091@gmail.com

Article History

Received: 25 June 2026 Revised: 10 July 2026 Accepted: 03 August 2026 Available Online: 07 August 2026

Abstract. Solar cells are considered a potential sustainable device for generating electricity from sunlight. However, the cost of commercial silicon based solar cells is high due to a complex manufacturing process. The halide double perovskite (HDP) solar cell provides high power conversion efficiency (PCE) at a lower fabrication cost due to their tunable optoelectronic properties and the inexpensive materials involved in the fabrication of the device. The basic structure of the solar cell contains the window layer, the electron transport layer (ETL), the absorber layer, and the hole transport layer (HTL). We have investigated the performance of Ga_2CeCl_6 based thin film solar cell (TFSC) numerically using SCAPS-1D (Solar Cell Capacitance Simulator). The structure of the device is ITO/C60/Ga_2CeCl_6/CZTS where ITO (indium tin oxide), C60, Ga_2CeCl_6 and CZTS (copper zinc tin sulfide) are the window layer, ETL, absorber layer, and HTL respectively. Various factors affect the performance of the TFSC, such as the thickness of different layers, the concentration of dopants, defects, operating temperature, series resistance, shunt resistance, and so on. These quantities are varied in a certain range, and their effects on the solar cell parameters such as open-circuit voltage (V_{OC}), short-circuit current density (J_{SC}), fill factor (FF), and PCE are obtained from simulation. The optimum values for those quantities are implemented to design a cost effective and high performing TFSC device. For the optimized Ga_2CeCl_6 based TFSC, the values of V_{OC}, J_{SC}, FF, and PCE are 1.2 V, 31 $mAcm^{-2}$, 89%, and 33.34%, respectively.

Key words. Halide double perovskite, High efficiency, Optimization, Solar cell

1. Introduction

Currently, more than 70% of electricity worldwide is generated by non-renewable sources of energy such as coal, natural gas, oil, nuclear energy, and so on [1,2]. There are several disadvantages of using these sources, such as emission of harmful gas into the atmosphere while burning the fossil fuels, depletion of sources due to extensive large usage, and increase in price due to scarcity and high market demand [3]. That is why non-renewable sources are considered unsustainable, and it is essential to develop the technology to generate electrical energy from renewable sources [4]. Among renewable sources of energy, wind, hydro and solar contribute primarily to the remaining 30% of electricity generation. There are several advantages of solar energy, such as high scalability, long lifespan, accessibility, and low impact on the environment [5].

The solar cell works on the principle of photovoltaic effect, by which sunlight is absorbed by the solar panels and converted into electrical energy [6]. Commercially, silicon is used as the semiconductor material to generate electrons and holes charge carriers [7]. They are further transported to the respective electrodes, and electric current is produced. The fabrication cost for silicon based solar cells is quite high [8]. Alternatively, halide double perovskites (HDP) are considered sustainable, environmentally friendly and low cost materials for solar cells [9]. They exhibit suitable optical, electronic, and photovoltaic properties to produce electricity from sunlight [10,11].

The general chemical formula of HDP is $A_2BB'X_6$ where A, B, B' are cations while X represents the halide anion [12]. Alghamdi et al. theoretically investigated the performance of a HDP based solar cell ($FTO/SnO_2/Cs_2PtI_6$/Spiro-OMeTAD/C) [13]. Power conversion efficiency (PCE) of 25.7% and quantum efficiency (QE) of 97.5% were obtained in the spectral range for the optimized device. In another theoretical study, Rb_2LiGaI_6, Cu_2O and TiO_2 are used as absorber layer, HTL and ETL respectively [14]. The optimized solar cell yielded PCE of 26.48% for the band gap of 1.13 eV of Rb_2LiGaI_6. The substitution of 5% Ga in the HDP $Cs_2AgBiBr_6$ reduces the band gap and improves the efficiency and stability of the solar cell [15]. Liu et al. have demonstrated other techniques such as vacuum treatment and interlayer engineering to enhance the performance of lead-free tin-based perovskite solar cell [16]. Various research groups have made efforts to improve the performance of HDP $Cs_2AgBiBr_6$ by doping rubidium [17], molybdenum [18], graphdiyne [19] and polypyrrole [20].

Band alignment of the absorber layer with the electron transfer layer (ETL) and hole transfer layer (HTL) is an important factor to consider for the fabrication of highly efficient device. Usually, ZnO, CdZnS, In_2O_3, IGTO, C60, Al_2O_3, WS_2, WO_3, TiO_2, PCBM, SnO_2, and LBSO are used as ETL [21] while Cu_2O, CBTS, CuSCN, P_3HT, PEDOT:PSS, GaAs, CdTe, PTAA, and Cu are used as HTL [22]. Mohandes et al. investigated the performance of Cs_2BiAgI_6 based thin film solar cell (TFSC) with ZnO/AZN as ETL [23]. In this work, eight devices with different HTL were manufactured and V_2O_5 was selected as HTL based on a quantitative analysis of device performance.

In this study, an optimized TFSC structure is investigated for the absorber layer of the Ga_2CeCl_6. First-principles calculations are performed by Rafiu et al. on Ga_2CeCl_6 to investigate its structural, electronic, thermoelectric, optical, mechanical, phonon stability, molecular dynamics, and photovoltaic properties. Their findings conclude that Ga_2CeCl_6 possesses stability, a tunable optoelectronic response, and strong photovoltaic performance [24]. It is placed between C60 ETL and copper zinc tin sulfide (CZTS) HTL. CZTS is a low-cost inorganic material which exhibits a tunable direct band gap and large absorption coefficient, making it a suitable material for HTL [25]. The performance of the device is examined with SCAPS-1D (Solar Cell Capacitance Simulator) software [26]. Parameters like thickness and carrier concentration of the window layer, ETL, absorber layer, and HTL are varied over a certain range and the corresponding variations in open-circuit voltage (V_{OC}), short-circuit current density (J_{SC}), fill factor (FF) and PCE are studied. In addition, the effects of factors such as operating temperature, defects, series, and shunt resistance on the performance of the solar cell are also examined. Finally, current density-voltage (J-V) characteristics, energy band diagram and QE are plotted for the optimized Ga_2CeCl_6 based TFSC.

2. Materials and Methodology

2.1 Numerical Simulation

Simulation of a model is often helpful to optimize the parameters for experimental work. We have used SCAPS-1D simulator to examine the performance of the solar cell under standard test conditions (STC). SCAPS-1D is developed at the University of Gent, Belgium [26]. It is an open-source TFSC simulator that gives very reliable results [27]. The software provides the option to add different materials along with their electronic and optical properties. The performance of the solar cell can be determined under STC. The effects of various factors such as defects, operating temperature, series, and shunt resistance, etc. on the device performance can also be studied by SCAPS-1D. SCAPS-1D simulator solves Poisson equation (Eq. 1) and continuity equation (Eq. 2) numerically for charge carriers in one dimension. It also solves the equations for the transport mechanism of the carriers by drift and diffusion processes according to Eqs. 3 and 4.

$$-\frac{\partial^2 \emptyset}{\partial x^2}=\frac{q}{\varepsilon}[p-n+N_D-N_A+\rho_p-\rho_n] \quad (1)$$

$$-\frac{\partial J_n}{\partial x}=\frac{\partial J_p}{\partial x}=G-R \quad (2)$$

$$J_n=D_n\frac{\partial n}{\partial x}+\mu_n n\frac{\partial \emptyset}{\partial x} \quad (3)$$

$$J_p=D_p\frac{\partial p}{\partial x}+\mu_p p\frac{\partial \emptyset}{\partial x} \quad (4)$$

where ϕ is electrostatic potential, q is charge, ε is electric permittivity, p is hole concentration, n is electron concentration, N_D is donor density, N_A is acceptor density, ρ_p is holes distribution, ρ_n is electrons distribution, J_n is electron current density, J_p is hole current density, G is generation rate, R is recombination rate, D_n and D_p are diffiusion coefficients, μ_n and μ_p are carrier mobilities.

2.2 Solar Cell Device Structure

An absorber layer absorbs the incident light and generates electron-hole pairs from the absorbed photons [28]. ETL and HTL extract electrons and holes from the absorber layer and facilitate their smooth transition to the front and back contacts, respectively. A transparent window layer is placed on top and is connected to the electrode.

Table 1. Input parameters for ITO, C60, Ga_2CeCl_6, and CZTS used in the simulation of solar cell.

	ITO	C60	Ga_2CeCl_6	CZTS
Thickness (nm)	100	100	800	1500
Band gap (eV)	3.3	1.7	1.733	1.45
Electron affinity (eV)	4.1	3.9	4.47	4.5
Dielectric constant	2	4.2	3.52	9
Conduction band density of states (cm^{-3})	2×10^{20}	8×10^{19}	2.5×10^{19}	2.2×10^{18}
Valence band density of states (cm^{-3})	1.8×10^{19}	8×10^{19}	1.5×10^{19}	1.8×10^{19}
Electron mobility ($cm^2V^{-1}s^{-1}$)	5	0.08	40	6
Hole mobility ($cm^2V^{-1}s^{-1}$)	7.5	3.5×10^{-3}	65	2
Donor density (cm^{-3})	1×10^{14}	1×10^{17}	1×10^{17}	0
Acceptor density (cm^{-3})	0	0	0	1×10^{16}
References	[29]	[30]	[24]	[31]

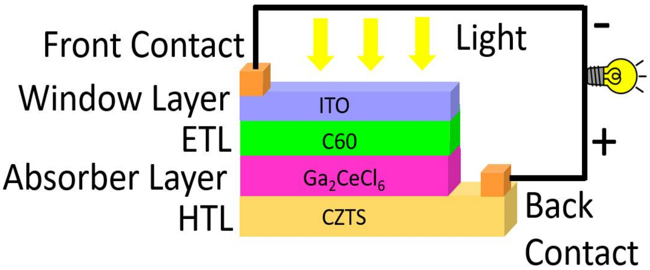

Figure 1. Schematic diagram of the structure of TFSC ITO/C60/Ga_2CeCl_6/CZTS.

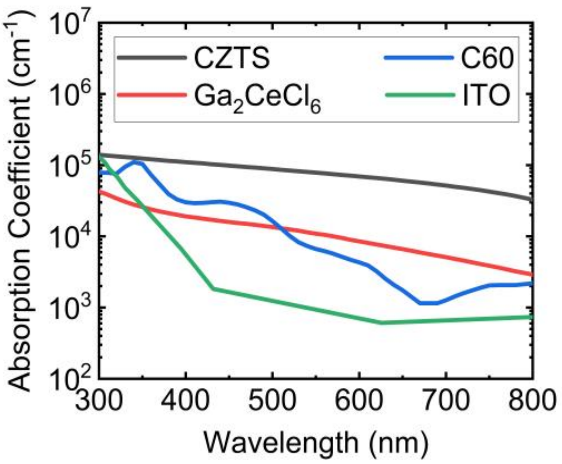

Figure 2. Absorption coefficients of CZTS, Ga_2CeCl_6, C60 and ITO over a wavelength range of 300 to 800 nm.

Schematic diagram of Ga_2CeCl_6 based TFSC is shown in Figure 1. Indium tin oxide (ITO) is a transparent conductive oxide (TCO) having a large band gap (3.3 eV) [29]. Most of the light passes through this layer without being absorbed. The thin ETL of C60 is placed below the window layer, which extracts the electrons and blocks the holes. Ga_2CeCl_6 absorbs the light that passes through the ETL and generates electron-hole pairs. The holes are extracted by CZTS HTL placed below the absorber layer. The holes are further collected by Cu metallic back contact. Similarly, electrons are collected by Cu metallic front contact. The electric current starts flowing through the load when applied across the terminals of the device. Under STC, the temperature is fixed at 300 K and the 1.5G AM solar spectrum with a power of 1000 Wm^{-2} is incident to the device window layer. The optoelectronic properties of the materials are given in Table 1 and absorption coefficients of the layers for wavelength range of 300 to 800 nm are plotted in Figure 2 [24,32-34]. Above 800 nm, the absorption of photons is significantly reduced by the layers.

3. Results and Discussion

3.1 Influence of Window Layer (ITO) Thickness on Device Performance

The light is incident on the window layer of the solar cell. It has low absorption and high transparency in the wavelength range of the solar spectrum [31]. When light is absorbed by the absorber layer, charge carriers, such as electrons and holes, are generated. The electrons move towards the ETL and further they pass through the window layer. They contribute to current flow when they are transferred through the front contact. The contact with the window layer should be stable to facilitate the flow of electrons and minimize series resistance [35]. A thicker window layer may be responsible for poor device efficiency by increasing series resistance. Optimization of the thickness of the window layer is essential for the overall performance of the device.

ITO is selected as the window layer for the Ga_2CeCl_6 based TFSC. The solar cell parameters V_{OC}, J_{SC}, FF, and PCE are plotted against the ITO thickness as shown in Figure 3.

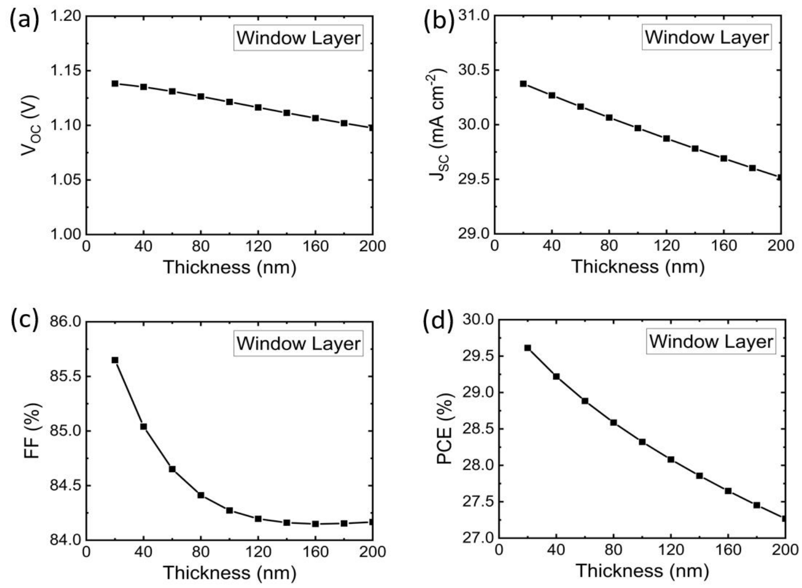

Figure 3. Effect of thickness of window layer (ITO) on solar cell parameters. (a) V_{OC}, (b) J_{SC}, (c) FF and (d) PCE.

All parameters have decreased while increasing the thickness of the layer from 20 to 200 nm. A decrease in J_{SC} implies that some of the photons are absorbed by ITO. This reduces the light reaching the absorber layer and hence the generation of electron-hole pairs is affected. V_{OC} is also affected, as the rate of electron-hole recombination is higher for a thicker layer. FF and PCE are also reduced, implying poor device performance due to thicker ITO. A thin ITO layer is suitable for Ga_2CeCl_6 based TFSC and the optimum thickness of ITO is 50 nm.

3.2 Influence of ETL (C60) Thickness on Device Performance

The electrons generated at the absorber layer from the absorbed photons are transferred to the front contact for the production of electricity. The transition of electrons becomes smooth with the help of ETL [36]. There are certain properties that are exhibited by the ETL such as proper band alignment with the window layer and the absorber layer [37]. Otherwise, the recombination of an electron-hole pairs at the interface deteriorates the performance of the solar cell. A thicker ETL reduces the recombination loss, whereas it may increase the absorption of light within the layer. The photons reaching the absorber layer would decrease as a result of thicker ETL resulting in a poor efficiency. The thickness of the ETL is an important factor which determines the performance of the solar cell. The thickness of C60 ETL is increased from 50 to 600 nm and the solar cell parameters are plotted against the thickness as shown in Figure 4. J_{SC} has increased by a small amount, suggesting that more photons are absorbed to generate the charge carriers. A marginal change in V_{OC} indicates that the reverse saturation current remains the same even for a thicker layer of C60. FF and PCE are not significantly affected by the thickness of the C60 layer. Less material is required to deposit a thinner layer during the manufacturing process. A 200 nm thick C60 ETL would be suitable for the device.

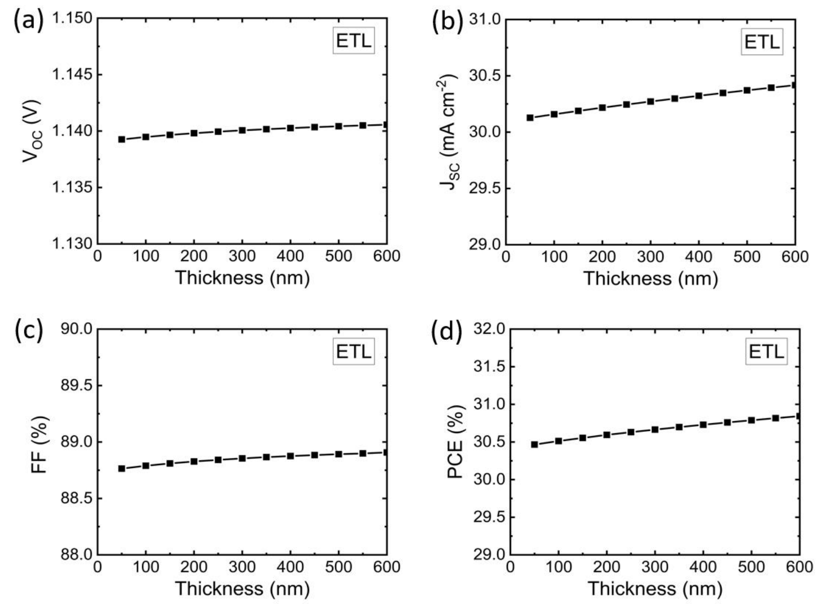

Figure 4. Effect of thickness of ETL (C60) on solar cell parameters. (a) V_{OC}, (b) J_{SC}, (c) FF and (d) PCE.

3.3 Influence of Absorber Layer (Ga_2CeCl_6) Thickness on Device Performance

Light is absorbed by the absorber layer to generate electron-hole pairs. Thus, poor absorption of light by the window layer and ETL result in higher efficiency of the solar cell. Electrons and holes move towards the front and back contacts for the production of electrical energy. The presence of additional layers such as ETL and HTL facilitate the smooth transition of electrons and holes, respectively. Abundances of charge carriers are generated if more number of photons are absorbed [38]. A thicker absorber layer is essential for higher photon absorption. However, the probability of recombination of electrons and holes also increases when the charge carriers have to travel longer distances within the absorber layer [39]. The series resistance is enhanced for thicker absorber layer. Both of these factors adversely affect the performance of the device.

Ga_2CeCl_6 is used as an absorber layer for the TFSC. The thickness of the absorber layer is varied from 0.5 to 5 μm as shown in Figure 5. The value of J_{SC} has increased with the thickness of the layer. More photons are absorbed by a thicker layer, which generates a large number of charge carriers. However, minor changes in V_{OC} suggest that most electron-hole pairs are recombined and heat is released during this process. Similarly, FF has also increased marginally. This may be due to the increase in series resistance occurring from the larger path length for the charge carriers. In general, the performance of the solar cell has improved with that of Ga_2CeCl_6 thickness, and 2 μm would be suitable thickness of the absorber layer for the Ga_2CeCl_6 based TFSC.

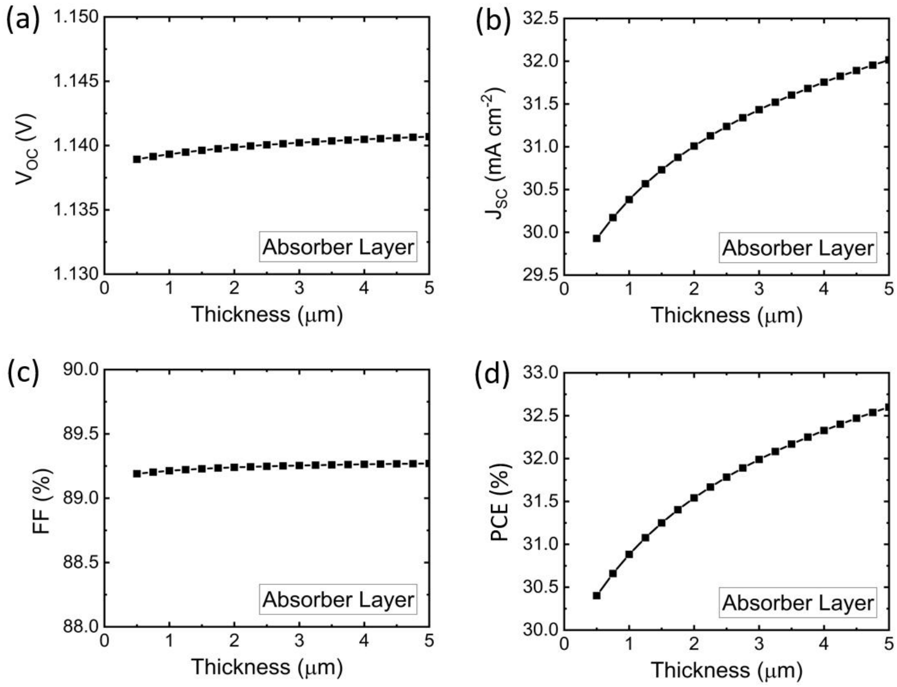

Figure 5. Effect of thickness of absorber layer (Ga_2CeCl_6) on solar cell parameters. (a) V_{OC}, (b) J_{SC}, (c) FF and (d) PCE.

3.4 Influence of HTL (CZTS) Thickness on Device Performance

The holes generated by the absorber layer reach the back contact for the production of electrical energy. For smooth transition of the holes, HTL is placed in between the absorber layer and the back contact electrode. The HTL also blocks the flow of electrons towards the back contact. A thin HTL increases the recombination loss, while a thick HTL increases the series resistance [40]. The thickness of the CZTS HTL ranges from 0.5 to 4.5 μm, as shown in Figure 6. A rapid increase in J_{SC} has been observed with that of the thickness of CZTS. More electron-hole pairs are generated in the device as a result of the absorption of photons even by the CZTS layer. V_{OC} remains unchanged with increasing thickness of CZTS. Most of the generated charge carriers must be recombined during the migration to the respective front and back contacts. A small increase in the FF with that of the CZTS thickness suggests that the series resistance offered by the thicker CZTS layer has not increased significantly. PCE has also increased, and the rate of increase is higher until the thickness of CZTS reaches 2 μm. For this thicker layer, a smaller increase in PCE is observed. The above analysis suggests that 2 μm is an optimum thickness of CZTS for the Ga_2CeCl_6 based TFSC.

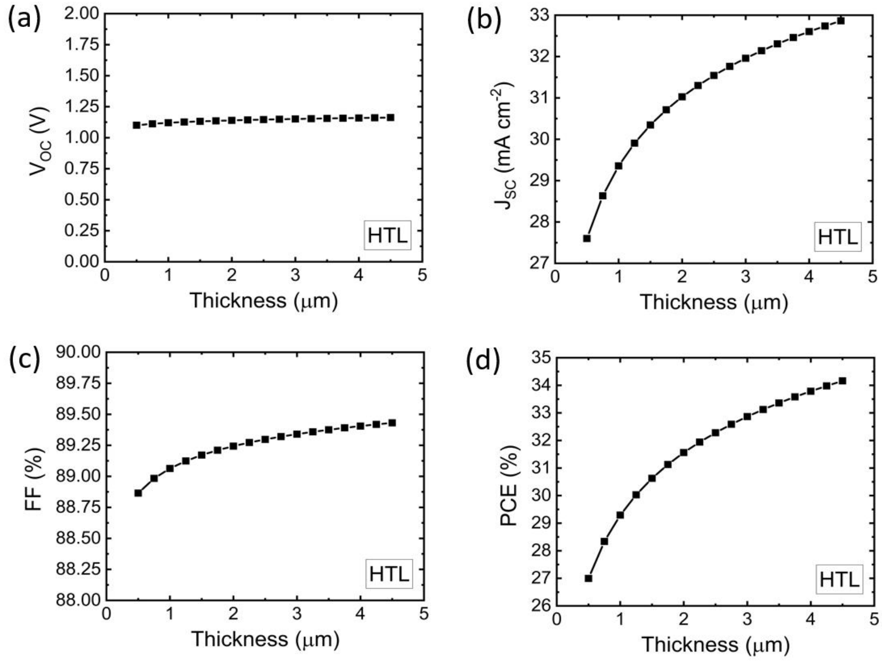

Figure 6. Effect of thickness of HTL (CZTS) on solar cell parameters. (a) V_{OC}, (b) J_{SC}, (c) FF and (d) PCE.

3.5 Influence of Window Layer (ITO) Donor Density on Device Performance

Donor charge carriers are added to the window layer of the solar cell. The purpose of the window layer is to transmit the light and smoothly transfer the electrons generated by the absorber layer to the front contact electrode. Increasing the carrier concentration could alter the band gap so that the recombination loss is reduced. However, a high donor density may adversely affect the performance of the solar cell [40]. ITO is used as a window layer for a Ga_2CeCl_6 based TFSC. The concentration of donor atoms in ITO is varied from 10^{10} to 10^{19} cm^{-3} and its effects on the solar cell parameters are plotted as shown in Figure 7. The V_{OC} remains unaffected by this variation in the donor density of ITO. The recombination of electron-hole pairs has not been influenced by increasing the donor density of ITO. For a lower donor density, J_{SC} remains the same, whereas it has increased sharply for a higher donor density above 10^{18} cm^{-3}. The presence of donor atoms in high concentration increases the generation of electron-hole pairs [40]. However, FF has increased with that of donor density. The series resistance of the solar cell has been reduced by increasing the donor density of ITO. However, a large concentration of donor atoms may have acted as defects and this leads to the saturation in the FF at higher donor density [41]. Similar effects have also been observed for the PCE of the solar cell. The 10^{14} cm^{-3} donor density for the ITO window layer of Ga_2CeCl_6 based TFSC can be implemented to improve the performance of the device.

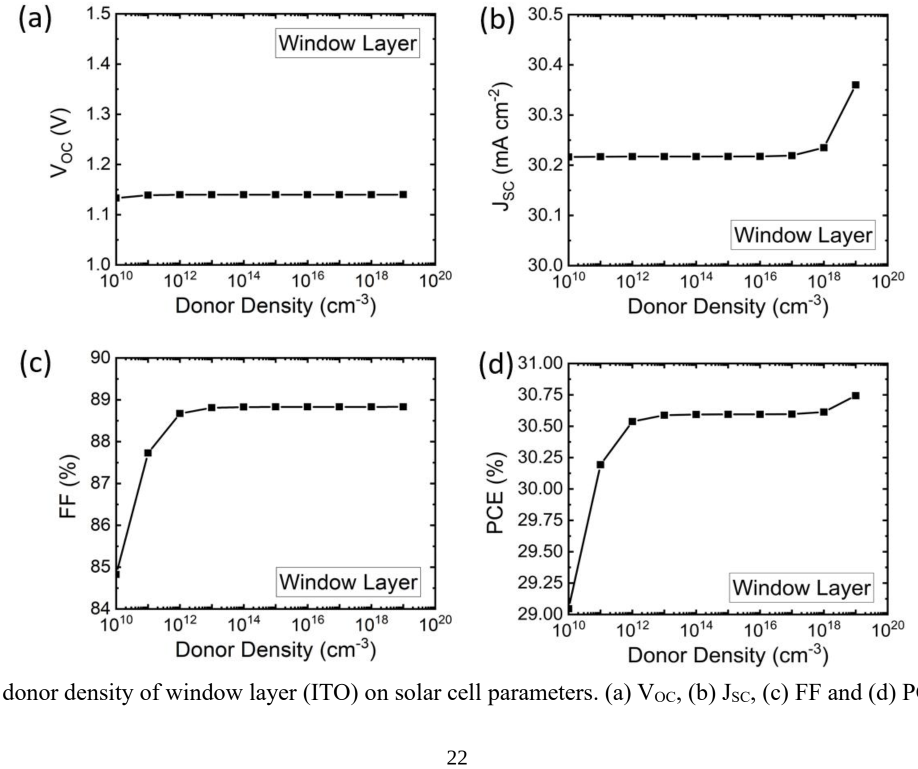

Figure 7. Effect of donor density of window layer (ITO) on solar cell parameters. (a) V_{OC}, (b) J_{SC}, (c) FF and (d) PCE.

3.6 Influence of ETL (C60) Donor Density on Device Performance

The role of ETL is to facilitate the charge extraction and smoothen the transition of electrons from the absorber layer towards the window layer. When the donor density in ETL is high, the presence of electrons increases the electric field across the region. The electrons move smoothly without contributing to the recombination loss. The series resistance also decreases as a result of the presence of a large number of electrons [40]. The donor density of C60 ETL has been increased from 10^{14} to 10^{23} cm^{-3} as shown in Figure 8. J_{SC} remains the same with this increase in concentration of the dopants, while a small decrease in V_{OC} has been observed for donor density of the C60 layer greater than 10^{20} cm^{-3}. FF has increased from 87.5% to 89.25% since the presence of dopants reduces the series resistance of the device. However, the dopants start to behave as defects if their concentration is too high. The optimum donor density of the C60 ETL would be 10^{20} cm^{-3} for the Ga_2CeCl_6 based TFSC.

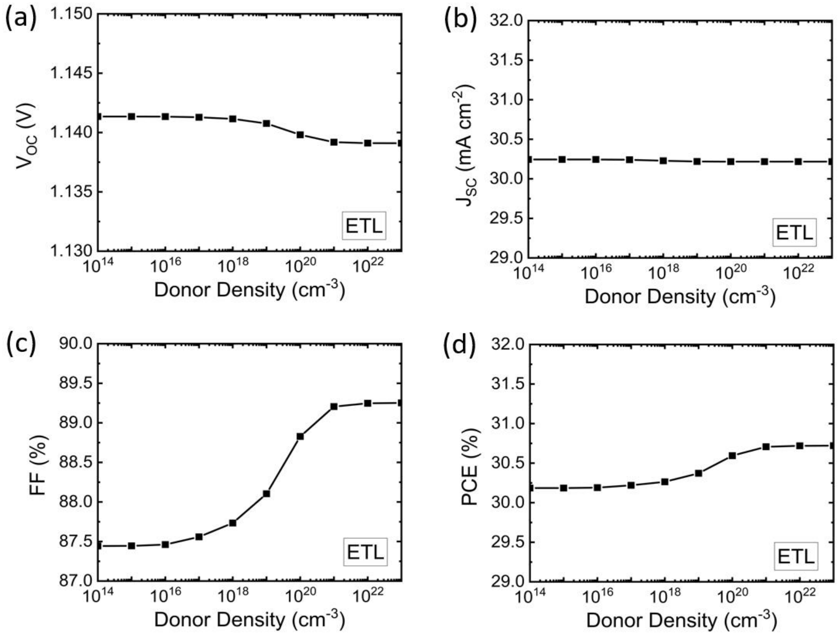

Figure 8. Effect of donor density of ETL (C60) on solar cell parameters. (a) V_{OC}, (b) J_{SC}, (c) FF and (d) PCE.

3.7 Influence of Absorber Layer (Ga_2CeCl_6) Donor Density on Device Performance

Charge carriers such as electrons and holes are extracted from the absorber layer as a result of the absorption of incoming radiation. If the donor density is too high, the dopants start behaving like defects and thus the efficiency of the solar cell is reduced [38]. A moderate increase in donor density changes the band gap and band alignment with the ETL and HTL. It helps in the smooth transition of electrons and holes towards ETL and HTL respectively. In this way, the performance of the solar cell is enhanced. An optimum donor density in the absorber layer plays a significant role for the device. The donor density of Ga_2CeCl_6 absorber layer is increased from 10^{14} to 10^{23} cm^{-3} and the parameters of the solar cell are plotted against the donor density as shown in Figure 9. Both V_{OC} and J_{SC} have been charged marginally, implying that the concentration of dopants in Ga_2CeCl_6 has not affected the rate of charge carrier generation and the recombination process. However, FF has increased from 88.5% to 89.25% with the increase in donor density from 10^{14} to 10^{17} cm^{-3}. PCE almost remains the same as that of donor density. The optimum donor density of Ga_2CeCl_6 is 10^{17} cm^{-3} for the device.

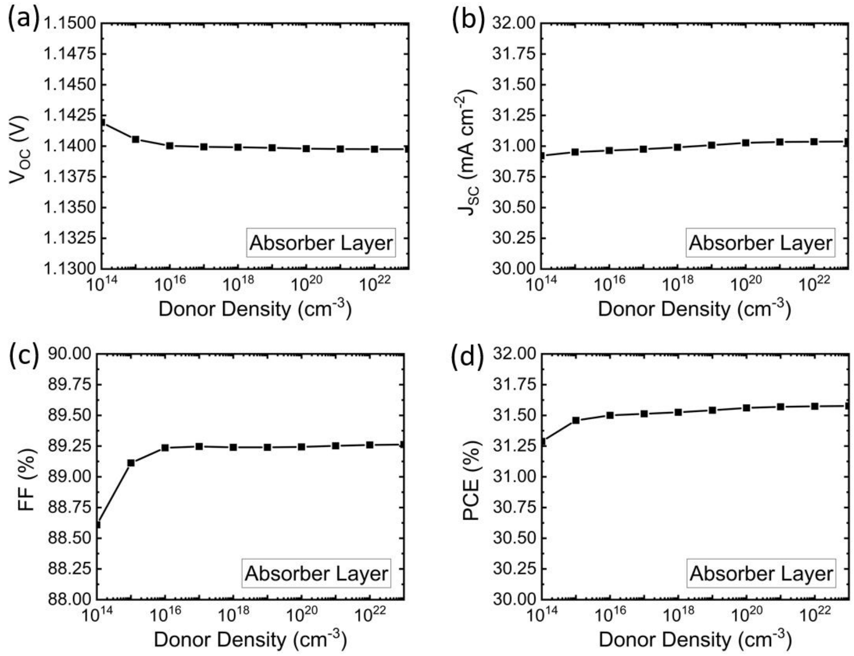

Figure 9. Effect of donor density of absorber layer (Ga_2CeCl_6) on solar cell solar cell parameters (a) V_{OC}, (b) J_{SC}, (c) FF and (d) PCE.

3.8 Influence of HTL (CZTS) Acceptor density on Device Performance

The HTL is doped with acceptor charge carriers, increasing the concentration of holes in the layer. It is used to move the holes generated by the absorber layer to the back contact. Adding holes to the HTL increases the charge concentration, thus reducing the series resistance of the device. It also decreases the recombination loss by increasing the number of holes present in the layer. The CZTS present in the device acts as an HTL for the Ga_2CeCl_6 based TFSC. It behaves as a p-type material and the concentration of dopants is varied from 10^{14} to 10^{23} cm^{-3} as shown in Figure 10. All of the performance parameters of solar cells are affected by the acceptor density of CZTS. The value of J_{SC} decreases with that of the acceptor density until it becomes saturated above 10^{19} cm^{-3}. This implies that a lesser number of charge carriers are generated as the concentration of dopants increases. However, V_{OC} has continuously increased with acceptor density. The reverse saturation current increases with the presence of a larger number of holes and suppression in the recombination process. Initially, the FF has increased rapidly with the acceptor density of the holes. The series resistance has been reduced by the presence of more acceptor atoms. PCE has been affected by the acceptor density as shown in Figure 10(d). However, a very large concentration may cause the acceptor atoms to behave like defects in the layer and thereby increase the series resistance of the device [38]. An acceptor density of 10^{20} cm^{-3} in the HTL is suggested for the optimized solar cell.

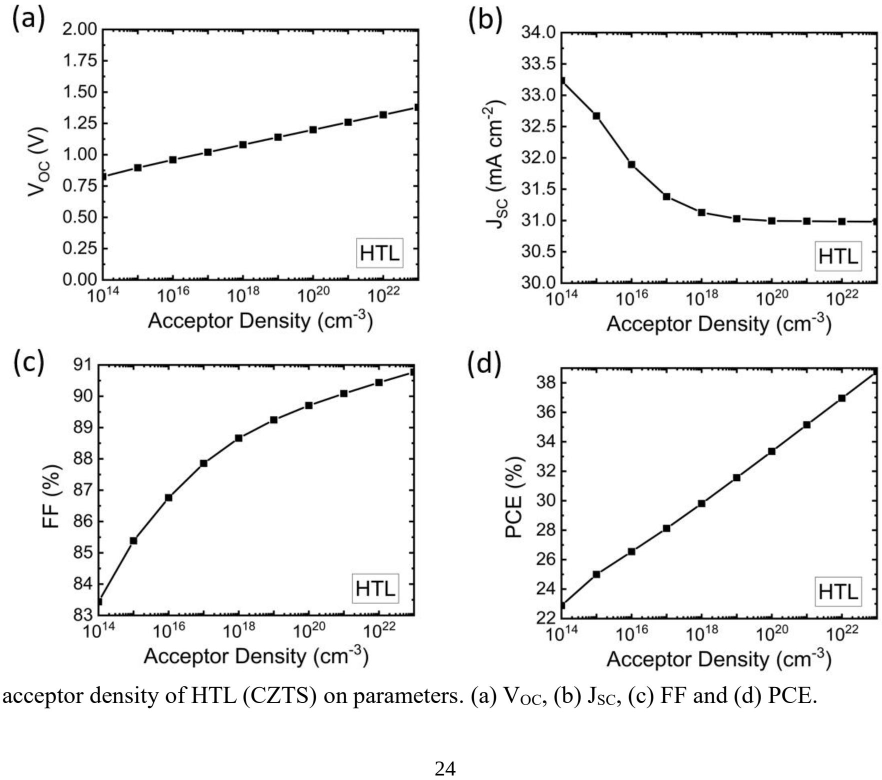

Figure 10. Effect of acceptor density of HTL (CZTS) on parameters. (a) V_{OC}, (b) J_{SC}, (c) FF and (d) PCE.

3.9 Influence of Operating Temperature on Device Performance

Exposure of a solar cell to sunlight leads to an increase in its temperature above 300 K. Higher temperature affects the performance of the device. The band gap of the layer decreases with an increase in temperature [42]. A smaller band gap increases the recombination rate of electron-hole pairs. It further increases the reverse saturation current and significantly reduces V_{OC} [43]. The generation of electron-hole pairs is marginally affected by the increase in the temperature of the solar cell. The total output power of the device decreases due to the drop in V_{OC}. The performance of the Ga_2CeCl_6 based TFSC is examined for a range of operating temperature from 290 to 420 K as shown in Figure 11. A continuous drop in V_{OC} occurs with the increase in temperature, whereas J_{SC} remains constant for this variation. The process of electron-hole pairs recombination dominates at higher operating temperatures, and it degrades the performance of the device [44]. The continuous drop in FF and PCE can be reduced by operating the device nearly at room temperature.

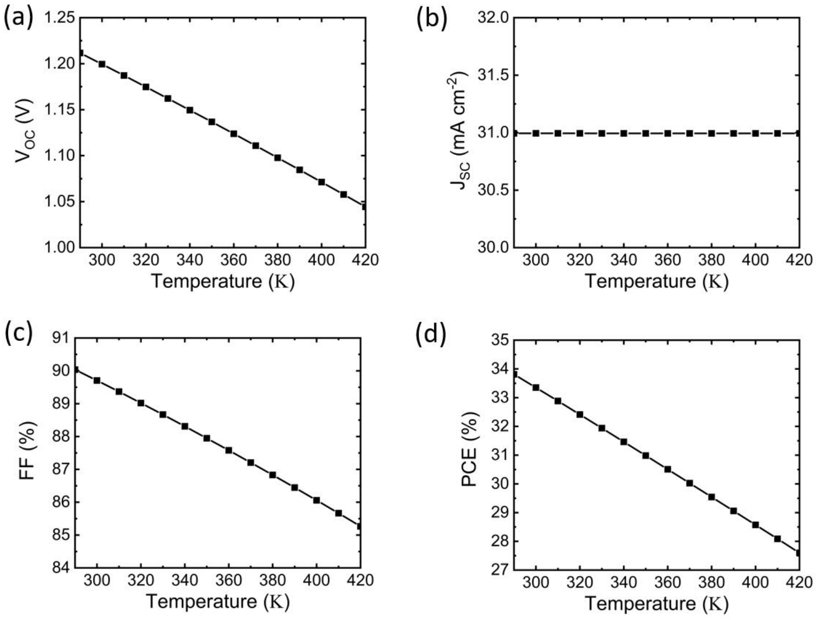

Figure 11. Effect of operating temperature on solar cell parameters. (a) V_{OC}, (b) J_{SC}, (c) FF and (d) PCE.

3.10 Influence of Series Resistance on Device Performance

Series resistance arises in a solar cell at front and back contacts of the device. The interfaces at various layers, such as the window layer, the ETL, the absorber layer, and the HTL, also contribute to the series resistance [45]. For an ideal solar cell, series resistance is considered as zero. However, in reality, it is unavoidable, and its presence reduces the performance of the device by increasing the voltage drop [38]. In our work, series resistance is varied from 10^{-6} to 10^{7} Ω cm^2 as shown in Figure 12 and solar cell parameters such as V_{OC}, J_{SC}, FF and PCE are calculated. The solar cell behaves as an ideal device for lower series resistance up to 0.1 Ω cm^2. The voltage drop across the series resistance increases drastically above 1 Ω cm^2. Unlike V_{OC}, J_{SC} has been reduced while increasing the series resistance. The generation of electron-hole pairs in the solar cell is influenced by the lower absorption of photons at the absorber layer. It is suggested to have proper metallic contacts for both electrodes and minimize interfacial defects during manufacturing processes.

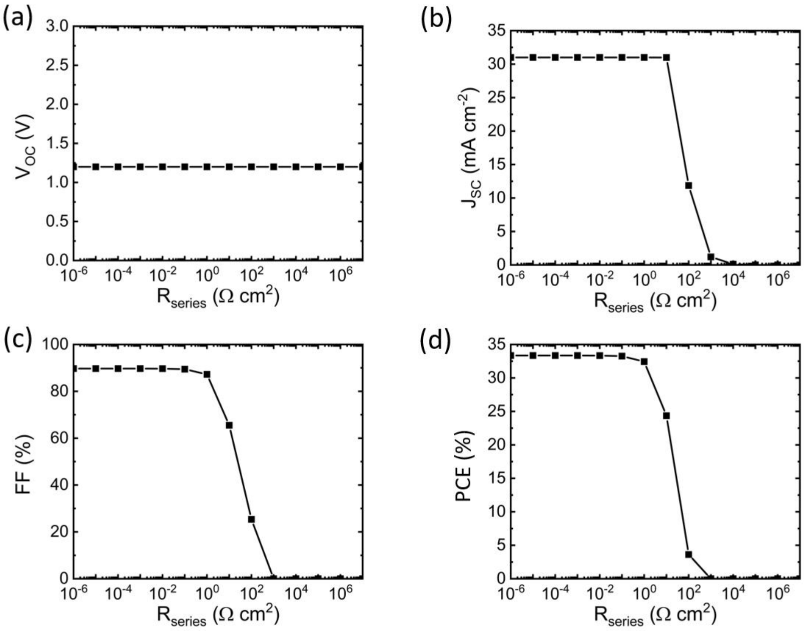

Figure 12. Effect of series resistance on solar cell parameters. (a) V_{OC}, (b) J_{SC}, (c) FF and (d) PCE.

3.11 Influence of Shunt Resistance on Device Performance

The defects present in various layers contribute to the shunt resistance of the solar cell. It arises during the manufacturing processes of various layers of the device [46]. For an ideal solar cell, infinite shunt resistance is considered. This obstructs the flow of current through the resistor, and the current passes completely through the device [38]. Thus, a higher shunt resistance is a favorable condition for a good performance of the device. The shunt resistance is varied from 10^{-1} to 10^{6} Ω cm^2 for the Ga_2CeCl_6 based TFSC as shown in Figure 13. J_{SC} is not affected by the shunt resistance of the device since electron-hole pairs are generated by the absorption of photons. However, V_{OC} is reduced to low voltage for a smaller shunt resistance below 100 Ω cm^2. The recombination process of electron-hole pairs increases due to the presence of defects, and it results in lower shunt resistance. FF and PCE are also reduced to lower values for a smaller shunt resistance. The shunt resistance should be maintained above 10^4 Ω cm^2 for optimal performance.

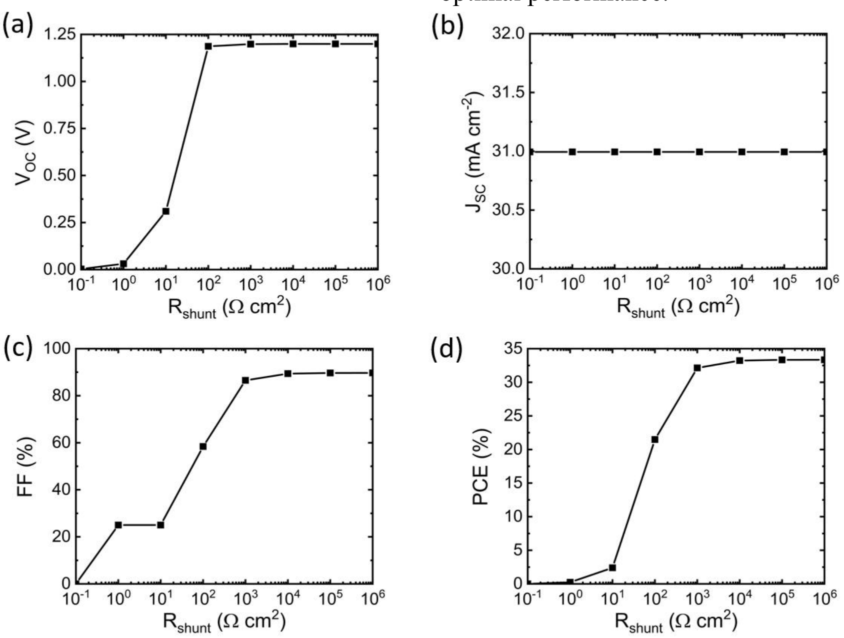

Figure 13. Effect of shunt resistance on solar cell parameters. (a) V_{OC}, (b) J_{SC}, (c) FF and (d) PCE.

3.12 Influence of Absorber Layer (Ga_2CeCl_6) Defect Density on Device Performance

Various processes such as photon absorption, generation of electron-hole pairs, and recombination of charge carriers are affected due to the presence of defects in the device [23]. A higher defect density in the layers degrades the performance of the solar cell. These defects act as a recombination center, which reduces the lifespan of the charge carriers. Electrons and holes recombine after traveling a shorter path in the device. The effects of defect density on the parameters of the solar cell are shown in Figure 14. The defect density of Ga_2CeCl_6 absorber layer is varied from 10^{11} to 10^{20} cm^{-3}. J_{SC} has decreased from 30 to 10 mA cm^{-2} for a defect density greater than 10^{17} cm^{-3}. The photons are not effectively absorbed by Ga_2CeCl_6 to generate electron-hole pairs. V_{OC} remains almost constant even for high defect density. A small decrease in V_{OC} is observed for a defect density greater than 10^{19} cm^{-3}. The FF does not change until the defect density is 10^{17} cm^{-3}. A sudden fall in FF is observed beyond this concentration of defects in the layer. However, PCE decreases significantly from 33% at a defect density higher than 10^{14} cm^{-3}. The stability of the absorber layer is a crucial factor affecting the performance of the solar cell. It is suggested to maintain the defect density of the absorber layer below 10^{13} cm^{-3} for the optimum performance of Ga_2CeCl_6 based TFSC.

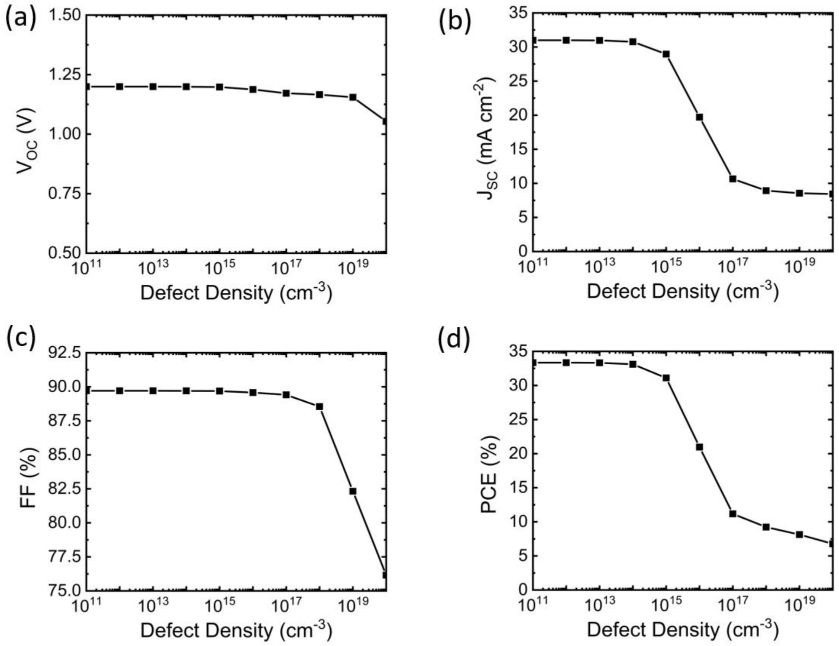

Figure 14. Effect of defect density of Ga_2CeCl_6 on solar cell parameters. (a) V_{OC}, (b) J_{SC}, (c) FF and (d) PCE.

3.13 Band Diagram, J-V Characteristics and QE of Optimized Device

The light incident at the window layer passes through it and is finally absorbed at the absorber layer. Thus, the window layer has a large band gap, whereas the band gap of the absorber layer matches well with the solar spectrum. Holes and electrons are generated at the absorber layer and are further transported to the corresponding back and front contacts. The charge carriers can be transported smoothly if there is minimal band offset at the interface [37]. The holes are extracted by HTL and move towards the back contact. The offset of the valence bands between the HTL and the absorber layer affects the extraction of the holes. In case of larger misalignment of the bands at the interface, recombination of charge carriers takes place, which reduces the performance of the device.

Similarly, electrons are extracted by ETL and transferred to the front contact after passing through the window layer. Conduction band alignment of the absorber layer and ETL at the interface is essential for smooth transition of electrons. A large offset of their valence bands at the interface blocks the movement of holes towards the front contact [37]. Poor band alignment at the interfaces causes the recombination of electron-hole pairs, which decreases the V_{OC} of the solar cell. CZTS, Ga_2CeCl_6, C60 and ITO are the HTL, absorber layer, ETL, and window layer of the device, respectively. The conduction band, valence band, band gap and the thickness of these layers for the optimized solar cell structure are shown in Figure 15. ITO allows most of the light in the solar spectrum to pass through due to its large band gap of 3.3 eV. The conduction bands of Ga_2CeCl_6 and C60 are properly aligned, facilitating smooth migration of electrons to the front contact electrode.

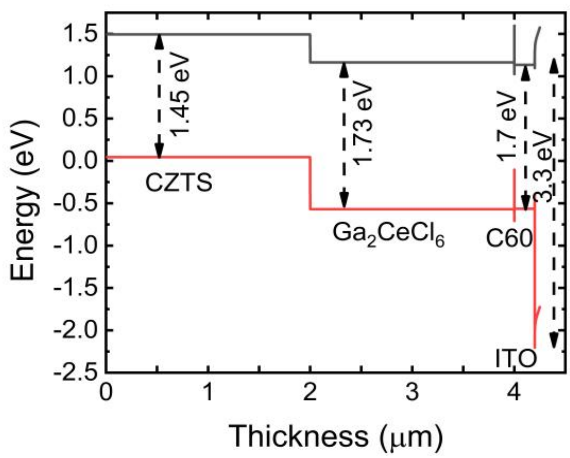

Figure 15. Energy band diagram of optimized Ga_2CeCl_6 based solar cell.

The QE is the ratio between the number of charge carriers collected at the electrodes and the number of photons incident at the solar cell. At a certain wavelength, QE is considered 100% if all photons emitted at that wavelength are absorbed, resulting in the production of an electric current. In this way, this parameter is used to measure the spectral response of the solar cell. Figure 16 shows the J-V characteristics and QE for the Ga_2CeCl_6 based TFSC with the optimized parameters. The QE is very high (above 95%) in the wavelength range of 400 to 800 nm. The optimization process is discussed above, and the optimized values are given in Table 2.The optimum values for the thickness of ITO, C60, Ga_2CeCl_6 and CZTS are 50, 200, 2000 and 2000 nm, respectively. The donor density for ITO, C60, and Ga_2CeCl_6 are 10^{14}, 10^{20}, and 10^{17} cm^{-3}, respectively, while the acceptor density for CZTS is 10^{20} cm^{-3}. Room temperature, defect density below 10^{13} cm^{-3} for Ga_2CeCl_6, series resistance of 0.1 Ω cm^2 or lower and higher shunt resistance above 10^4 Ω cm^2 are suitable conditions for the device. The solar cell parameters V_{OC}, J_{SC}, FF and PCE for the optimized device under favorable conditions are 1.2 V, 31 mA cm^{-2}, 89% and 33.34% respectively. These parameters for different HDPs are further compared with the Ga_2CeCl_6 based TFSC, given in Table 3.

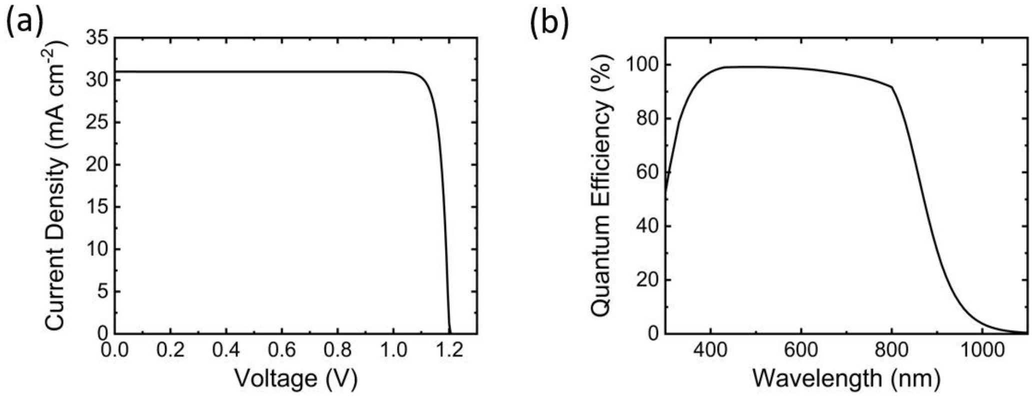

Figure 16. J-V characteristics and QE for the Ga_2CeCl_6 based TFSC with the optimized parameters. (a) After the process of optimization, the current density-voltage (J-V) characteristics of the device show a high FF with V_{OC} = 1.2 V, and J_{SC} = 31 mA cm^{-2}; (b) The quantum efficiency (QE) of the optimized Ga_2CeCl_6 based TFSC is above 95% in the wavelength range of 400 to 800 nm.

Table 2. Optimized values of various factors obtained from the simulation of Ga_2CeCl_6 based TFSC.

	Optimized values
Thickness of window layer (ITO)	50 nm
Thickness of ETL (C60)	200 nm
Thickness of absorber layer (Ga_2CeCl_6)	2000 nm
Thickness of HTL (CZTS)	2000 nm
Donor density of window layer (ITO)	1 x 10^{14} cm^{-3}
Donor density of ETL (C60)	1 x 10^{20} cm^{-3}
Donor density of absorber layer (Ga_2CeCl_6)	1 x 10^{17} cm^{-3}
Acceptor density of HTL (CZTS)	1 x 10^{20} cm^{-3}
Operating temperature for the device	Near room temperature
Series resistance of the device	Below 0.1 Ω cm^2
Shunt resistance of the device	Above 1 x 10^4 Ω cm^2
Defect density of absorber layer (Ga_2CeCl_6)	Below 1 x 10^{13} cm^{-3}

Table 3. Comparison of solar cell parameters for various device structures obtained from theoretical studies.

	V_{OC} (V)	**J_{SC} (mA cm^{-2})**	**FF (%)**	**PCE (%)**	**References**
ITO/WS_2/$Cs_2AgSbBr_6$/CBTS	1.037	25.20	80.46	21.40	[47]
ITO/ZnO/AZO/Cs_2BiAgI_6/V_2O_5	1.322	23.84	86.3	27.2	[23]
FTO/TiO_2/Rb_2LiGaI_6/Cu_2O	0.89	31.87	79	26.48	[14]
ITO/WS_2/Dy_2NiMnO_6/CFTS	0.741	44.67	80.67	26.72	[48]
ITO/$BaSnO_3$/$K_2CuBiBr_6$/NiO	0.98	29.20	55.88	14.70	[49]
ITO/C60/Ga_2CeCl_6/CZTS	1.2	31	89	33.34	This work

4. Conclusions

In this work, SCAPS-1D solar cell simulator software is used to optimize the performance of Ga_2CeCl_6 based TFSC. The structure of the device is ITO/C60/Ga_2CeCl_6/CZTS where ITO, C60, Ga_2CeCl_6, and CZTS are the window layer, the ETL, the absorber layer and the HTL respectively. The parameters of the solar cell V_{OC}, J_{SC}, FF and PCE are evaluated while varying various quantities, such as the thickness of the layers, the concentration of dopants in the layers, the operating temperature, the defect density of the Ga_2CeCl_6, series, and the shunt resistance of the device. Finally, the energy band diagram, the J-V characteristic, and the QE curves are plotted for the optimized solar cell. The genration of electron-hole pairs by photon absorption occurs mainly in the absorber layer, and this property is quantified by the value of J_{SC}. For the Ga_2CeCl_6 based TFSC, J_{SC} is significantly affected by the thickness of ITO, Ga_2CeCl_6 and CZTS, acceptor density of CZTS, the series resistance and the defect denisty of Ga_2CeCl_6. The reverse saturation current existing in the device is affected by the recombination process of electron-hole pairs, and the V_{OC} of the device is estimated to understand this current. Quantities such as the acceptor density of CZTS, the operating temperature, and the shunt resistance significantly affect the parameter V_{OC} of Ga_2CeCl_6 based TFSC. FF also depends on the generation of charge carriers and the reverse saturation current. In addition, the quality of the solar cell and the presence of series resistance across the device are captured by its FF. The value of FF is mostly affected by the thickness and donor density of ITO, donor density of C60, acceptor density of CZTS, operating temperature, defect density of Ga_2CeCl_6, series, and shunt resistance. PCE captures the overall performance of the solar cell, and it is affected by all the quantities considered in this study. These factors should be chosen very precisely before fabricating the real device, and such types of simulation works are very helpful in optimizing the device parameters. The optimum values obtained for V_{OC}, J_{SC}, FF and PCE are 1.2 V, 31 mA cm^{-2}, 89%, and 33.34%, respectively.

Acknowlegements

The author is thankful to Dr M. Burgelman of the University of Gent, Belgium for providing the SCAPS-1D software.

Declaration of Generative AI

No generative AI tools were used in the preparation of this manuscript.

Conflicts of Interest

The author declares that he has no conflict of interest.

Author Contributions

Sumeet Kumar: conceptualization, methodology, software, validation, data curation, writing, and reviewing.

References

[1] A. Karaeva, E. Magaril, I. Rukavishnikova. Comparative analysis of national decarbonization policies: Is it possible to achieve carbon neutrality by 2050? WIT Transactions on Ecology and the Environment, 2023, 261, 35-47. DOI: 10.2495/ESUS230041

[2] R. Das, T. Kandil, A. Harris, B. Herron, E.J. Magnante. A hybrid learning framework for national level power generation forecasting of different energy sources including renewable energy and fossil fuel. Energies, 2026, 19(6), 1564. DOI: 10.3390/en19061564

[3] M. Haque. Harmful impact of non-renewable resources on environment. Jatiya Kabi Kazi Nazrul Islam University, 2025. DOI: 10.13140/RG.2.2.35384.25600

[4] I. Khan, M. Sahabuddin. Chapter 1 - sustainability-concept and its application in the energy sector. Renewable Energy and Sustainability: Prospects in the Developing Economies, 2022, 1-21. DOI: 10.1016/B978-0-323-88668-0.00005-X

[5] S. Stevanovic, S. Stevanovic, R. Zivkovic. Adantages and disadvantages of solar-energy production and use. Journal of Agricultural Food and Environmental Sciences, 2022, 76(4), 65-70. DOI: 10.55302/JAFES22764065s

[6] P. Wurfel. Conversion of chemical energy into electrical energy. Physics of Solar Cells, 2005, 93-107. DOI: 10.1002/9783527618545.ch5

[7] A.S. Arul Prishya, M. Lalita Chopra. Comprehensive review on uses of silicon dioxide in solar cell. Materials Today: Proceedings, 2023, 72(3), 1471-1478. DOI: 10.1016/j.matpr.2022.09.348

[8] A. Singh, V. Umakanth, N. Tyagi, A.K. Baghel, S. Kumar. Comparative study of commercial crystalline solar cells. Results in Optics, 2023, 11, 100379. DOI: 10.1016/j.rio.2023.100379

[9] F. Ji, G. Boschloo, F. Wang, F. Gao. Challenges and progress in lead-free halide double perovskite solar cells. Solar RRL, 2023, 7(6), 2201112. DOI: 10.1002/solr.202201112

[10] D. Choudhary, M. Kaur, G. Sharma, R. Palsaniya, S. Loyalka, S. Singh, et al. Impact of halide variation on the optoelectronic properties of double perovskites. Scientific Reports, 2025, 15(1), 33629. DOI: 10.1038/s41598-025-98686-6

[11] Bhawna, A. Alam, M. Aslam. Halide double perovskites: Insights into structure, defects, and luminescence. ACS Applied Materials & Interfaces, 2026, 18(7), 10681-10724. DOI: 10.1021/acsami.5c20712

[12] C. Pareja-Rivera, D. Zugasti-Fernandez, P. Olalde-Velasco, D. Solis-Ibarra. Halide double perovskites. Halide Perovskite Semiconductors, 2024. DOI: 10.1002/9783527829026.ch5

[13] R.N.S. Alghamdi, E.I. Shalaan, A.O.M. Alzahrani. Scaps-1d simulation of lead free perovskite solar cells: Performance analysis and optimization. RSC Advances, 2026, 16(15), 13875-13885. DOI: 10.1039/d5ra08437g

[14] M. SK, M.T. Islam, Gourav. Exploring the structural, electronic, optical, transport, and photovoltaic properties of $Rb_2LiGa(Br/I)_6$ using DFT and SCAPS-1D simulations. Scientific Reports, 2024, 14(1), 24813. DOI: 10.1038/s41598-024-76593-6

[15] Ihtisham-ul-haq, M.I. Khan, A. Ullah, A. Mujtaba, B.S. Almutairi, W. Shahid, et al. Bandgap reduction and efficiency enhancement in $Cs_2AgBiBr_6$ double perovskite solar cells through gallium substitution. RSC Advances, 2024, 14(8), 5440-5448. DOI: 10.1039/d3ra08965g

[16] T. Liu, R. Nishikubo, A. Wakamiya, A. Saeki. Vacuum treatment and interface engineering enhance the efficiency and stability of tin halide perovskite solar cells. ACS Applied Energy Materials, 2026, 9(4), 2229-2238. DOI: 10.1021/acsaem.5c03794

[17] Z. Zhang, C. Wu, D. Wang, G. Liu, Q. Zhang, W. Luo, et al. Improvement of $Cs_2AgBiBr_6$ double perovskite solar cell by rubidium doping. Organic Electronics, 2019, 74, 204-210. DOI: 10.1016/j.orgel.2019.06.037

[18] Ihtisham-ul-haq, M.I. Khan, L.B. Farhat, H. Elhouichet, R.P. Patil. Enhancing efficiency of $Cs_2AgBiBr_6$ double perovskite solar cells through bandgap reduction by molybdenum doping. Journal of the Korean Ceramic

Society, 2025, 62(2), 359-369. DOI: 10.1007/s43207-025-00476-3
[19] S. Umer, M.I. Khan, A. Ullah, Ihtisham-ul-haq, M. Asad, Imen Kebaili, et al. Improving $Cs_2AgBiBr_6$ double perovskite solar cells through graphdiyne doping: A stride towards enhanced performance. Optical Materials, 2024, 156, 115896. DOI: 10.1016/j.optmat.2024.115896
[20] Ihtisham-ul-haq, M.I. Khan, A. Mujtaba, A. Ullah, B. Ali, M. Atif, et al. Enhancing efficiency in double perovskite solar cells through bandgap reduction via organic polymer doping. Results in Chemistry, 2025, 13, 101999. DOI: 10.1016/j.rechem.2024.101999
[21] H. Bencherif, L. Dehimi, N. Mahsar, E. Kouriche, F. Pezzimenti. Modeling and optimization of CZTS kesterite solar cells using TiO_2 as efficient electron transport layer. Materials Science and Engineering: B, 2022, 276, 115574. DOI: 10.1016/j.mseb.2021.115574
[22] M. Tarekuzzaman, K.I.F. Utsho. Advancing solar energy with Cs2TlAsI6 double halide perovskite: A simulation-driven approach for high-efficiency solar cell. Advanced Electronic Materials, 2025, 11(16), 00312. DOI: 10.1002/aelm.202500312
[23] A. Mohandes, M. Moradi. Achieving 27.20% efficiency for a lead-free double perovskite solar cell with all inorganic Cs2BiAgI6 using azo utl as a passivation layer. Materials Advances, 2025, 6(4), 1520-1539. DOI: 10.1039/d4ma01280a
[24] R. Rafu, K. Kriaa, M.S.H. Saikot, M.A. Rahman, I.A. Apon, N. Sfna, et al. Comprehensive first-principle analysis and device simulations of vacancy-ordered D2CeX6 double perovskites for high-efficiency lead-free solar cells. RSC Advances, 2025, 15(52), 44711-44748. DOI: 10.1039/d5ra07162c
[25] A.C. Piñón Reyes, R.C. Ambrosio Lázaro, K. Monfil Leyva, J.A. Luna López, J. Flores Méndez, A.H. Heredia Jiménez, et al. Study of a lead-free perovskite solar cell using CZTS as HTL to achieve a 20% PCE by SCAPS-1D simulation. Micromachines, 2021, 12(12), 1508. DOI: 10.3390/mi12121508
[26] M. Burgelman, P. Nollet, S. Degrave. Modeling polycrystalline semiconductor solar cells. Thin Solid Films, 2000, 361-362, 527-532. DOI: 10.1016/S0040-6090(99)00825-1
[27] A. Kowsar, M. Billah, S. Dey, S.C. Debnath, S. Yeakin, S.F.U. Farhad. Comparative study on solar cell simulators. 2019 2nd International Conference on Innovation in Engineering and Technology (ICIET), 2019, 1-6. DOI: 10.1109/ICIET48527.2019.9290675
[28] S. Souri, M. Marandi. Numerical modelling of the effect of the Ag: ZnSe BSF layer on the high performance of ZnSe/CdTe thin film solar cells by SCAPS-1D software. Optical and Quantum Electronics, 2023, 55(5), 397. DOI: 10.1007/s11082-023-04563-9
[29] S.H. Zyoud, M.G. Daher, M.M. Shabat. Enhancing the efficiency of thin film heterojunction solar cells with CIGS using alternative metal chalcogenide buffer layers: SCAPS-1D simulation software. 2023 8th International Engineering Conference on Renewable Energy & Sustainability (ieCRES), 2023, 1-4. DOI: 10.1109/ieCRES57315.2023.10209492
[30] M.H. Albelbeisi, A.M. Ahmed, M.G. Daher, M.A. Abdelkawy, M. Al-Hmoud, A. Hajjiah, et al. An analysis and design of perovskite-plasmonic solar cells employing tin FaSnI3 with various electron selective layers. Plasmonics, 2025, 20(12), 11761-11771. DOI: 10.1007/s11468-025-03238-3
[31] S.H. Zyoud, A.H. Zyoud, N.M. Ahmed, A.R. Prasad, S.N. Khan, A.F.I. Abdelkader, et al. Numerical modeling of high conversion efficiency FTO/ZnO/CdS/Mo thin film-based solar cells: Using SCAPS-1D software. Crystals, 2021, 11(12), 1468. DOI: 10.3390/cryst11121468
[32] N.M. Khusayfan, M.M. El-Nahass. Study of structure and electro-optical characteristics of indium tin oxide thin films. Advances in Condensed Matter Physics, 2013, 2013(1), 408182. DOI: 10.1155/2013/408182
[33] A.H.A. Jalaukhan, M.M.A. Hussein. Substrate temperature influence on optical properties of C60 thin films within the visible range. Iraqi Journal of Science, 2019, 60(5), 1006-1012. DOI: 10.24996/ijs.2019.60.5.10
[34] R. Ranjan, N. Anand, M.N. Tripathi, N. Srivastava, A.K. Sharma, M. Yoshimura, et al. SCAPS study on the effect of various hole transport layer on highly efficient 31.86% eco-friendly CZTS based solar cell. Scientific Reports, 2023, 13(1), 18411. DOI: 10.1038/s41598-023-44845-6
[35] S. Ghosh, T. Singh. Long term stability assessment of perovskite solar cell via recycling of metal contacts under ambient conditions. Materials Letters, 2022, 322, 132490. DOI: 10.1016/j.matlet.2022.132490
[36] R.K. Yadav, P.S. Pawar, R. Nandi, K.E. Neerugatti, Y.T. Kim, J.Y. Cho, et al. A quantitative study of SnSe thin film solar cells using SCAPS-1D and comparison with experimental results: A pathway towards 22.69% efficiency. Solar Energy Materials and Solar Cells, 2022, 244, 111835. DOI: 10.1016/j.solmat.2022.111835
[37] P. Schulz, L.L. Whittaker-Brooks, B.A. MacLeod, D.C. Olson, Y.L. Loo, A. Kahn. Electronic level alignment in inverted organometal perovskite solar cells. Advanced Materials Interfaces, 2015, 2(7), 1400532. DOI: 10.1002/admi.201400532
[38] R. Hosen, S. Sikder, M.S. Uddin, M.M. Haque, H. Mamur, M.R.A. Bhuiyan. Effect of various layers on improving the photovoltaic efficiency of Al/ZnO/CdS/CdTe/Cu2O/Ni solar cells. Journal of Alloys and Metallurgical Systems, 2023, 4, 100041. DOI: 10.1016/j.jalmes.2023.100041
[39] L.M. Pazos-Outon, T.P. Xiao, E. Yablonovitch. Fundamental efficiency limit of lead iodide perovskite solar cells. The Journal of Physical Chemistry Letters, 2018, 9(7), 1703-1711. DOI: 10.1021/acs.jpclett.7b03054
[40] A. Bag, R. Radhakrishnan, R. Nekovei, R. Jeyakumar. Effect of absorber layer, hole transport layer thicknesses, and its doping density on the performance of perovskite solar cells by device simulation. Solar Energy, 2020, 196, 177-182. DOI: 10.1016/j.solener.2019.12.014
[41] W.H. Nguyen, C.D. Bailie, E.L. Unger, M.D. McGehee. Enhancing the hole conductivity of spiro-ometad without oxygen or lithium salts by using spiro(tfsi)2 in perovskite and dye-sensitized solar cells. Journal of the American Chemical Society, 2014, 136(31), 10996-11001. DOI: 10.1021/ja504539w
[42] M. Asaduzzaman, A.N. Bahar, M.M. Rahman Bhuiyan, M.A. Habib. Impacts of temperature on the performance of CdTe based thin-film solar cell. IOP Conference Series: Materials Science and Engineering, 2017, 225(1), 012274. DOI: 10.1088/1757-899X/225/1/012274
[43] E. Karimi, S.M.B. Ghorashi. Simulation of perovskite solar cell with P3HT hole transporting materials. Journal of Nanophotonics, 2017, 11(3), 032510. DOI: 10.1117/1.JNP.11.032510
[44] F. Behrouznejad, S. Shahbazi, N. Taghavinia, H.P. Wu, E. Wei-Guang Diau. A study on utilizing different metals as the back contact of Ch3Nh3PbI3 perovskite solar cells. Journal of Materials Chemistry A, 2016, 4(35), 13488-13498. DOI: 10.1039/C6TA05938D
[45] W.F. Mohamed, M.A. Shehathah. The effect of the series resistance on the photovoltaic properties on In-doped CdTe(p) thin film homojunction structure. Renewable Energy, 2000, 21(2), 141-152. DOI: 10.1016/S0960-1481(00)00008-2

[46] C.H. Swartz, S.R. Rab, S. Paul, M.F.A.M. van Hest, B. Dou, J.M. Luther, et al. Measurement of band offsets and shunt resistance in CdTe solar cells through temperature and intensity dependence of open circuit voltage and photoluminescence. Solar Energy, 2019, 189, 389-397. DOI: 10.1016/j.solener.2019.07.057
[47] S.M.G. Mostafa, K.I.F. Utsho, M.S. Rahman, M. Tarekuzzaman, O. Alsalmi, M. Rasheduzzaman, et al. Device engineering and performance analysis of $Cs_2AgSbBr6$ perovskite solar cell using SCAPS-1D. Inorganic Chemistry Communications, 2025, 178, 114636. DOI: 10.1016/j.inoche.2025.114636
[48] N. Shahadath, M.A.B. Siddique, M. Tarekuzzaman, M.H. Ishraq, M.F. Rahman, A.M. Arfi, et al. Optimization of high efficiency lead-free double perovskite Dy2NiMnO6 (DNMO) for optimal solar cell renewable energy applications: A numerical SCAPS-1D simulation. New Journal of Chemistry, 2024, 48, 14336. DOI: 10.1039/d4nj02754j
[49] Jyoti, D. Muchahary. Numerical analysis of K2CuBiBr6 for enhanced solar cell performance potential. Modelling and Simulation in Materials Science and Engineering, 2025, 33, 045018. DOI: 10.1088/1361-651X/add94f